State-selective electron-capture calculations for *p*-Ar collisions in an independent many-electron model

T. Kirchner*
Institut für Theoretische Physik, TU Clausthal, Leibnizstraße 10, D-38678 Clausthal-Zellerfeld, Germany

M. Horbatsch†
Department of Physics and Astronomy, York University, Toronto, Ontario, Canada M3J 1P3

M. Keim‡ and H. J. Lüdde§
Institut für Theoretische Physik, Johann Wolfgang Goethe–Universität, Robert-Mayer-Straße 8, D-60054 Frankfurt/Main, Germany
(Received 1 July 2003; published 21 January 2004)

We extend previous calculations of many-electron processes in ion-atom collisions to the case of state-selective electron capture by protons from the K,L,M shells in argon at 1–200 keV/amu collision energies. The results are based on a time-dependent density functional theory framework and the basis generator method for the propagation of atomic orbitals. Impact-parameter-dependent probabilities are obtained from a statistical analysis. The results for capture to the H(K,L,M) shells are compared with experiments, and are found to agree with them much better than previous calculations. This serves as an indication that both a proper account of atomic structure and flexibility in the propagation of atomic orbitals are important.

DOI: 10.1103/PhysRevA.69.012708 PACS number(s): 34.50.Fa, 34.70.+e

I. INTRODUCTION

Multiple-electron processes in medium-energy collisions of ions with oxygen, neon, and argon targets have recently been investigated in a quantum mechanical framework [1–8]. This work is based on a time-dependent independent particle model (IPM) built upon the stationary optimized potential method (OPM) of density functional theory. Initially a frozen target potential was used, which is appropriate for high-energy collisions [1–4]. For intermediate energies, and especially below 200 keV/amu, it was shown that target response plays an important role when multiply charged projectile impact is considered [5–7]. For argon targets we found that response effects are noticeable even for proton impact [8].

At intermediate collision energies electron capture and ionization represent competing processes. A good calculation of the atomic orbital evolution thus requires one to take into account the electron continuum even if the focus is on excitation or capture. In the basis generator method (BGM) one accomplishes this task by starting with a substantial basis of exact target orbitals (e.g., the numerical eigenfunctions of the optimized effective potential used in the OPM [9]) and by assembling a hierarchy of states by repeatedly acting upon the eigenstates with powers of the projectile interaction. It has been demonstrated that this system-specific basis which changes with the internuclear separation is capable of representing adiabatic correlation diagrams. More importantly, the method correctly distributes the probability flux to capture and to ionization channels over a very wide range of collision energies from about 1 keV/amu to the highest energies that can be treated nonrelativistically. The basis does not include the traveling projectile states explicitly. Therefore, the calculation of state-specific capture channels represents a challenge for this approach.

Experiments on shell-specific and state-specific capture in *p*-Ar collisions have been carried out over quite some time, and while they are not all in perfect agreement, one can state that from an experimental point of view the basic processes such as total capture and capture to the H($n=2$) shell are understood at the factor-of-2 level or better. The situation is different for capture to the $n=3$ shell of hydrogen, where serious discrepancies remain, and no successful theoretical analysis of the situation has been achieved to date.

A recent calculation by Amaya-Tapia and co-workers [10] provided a first detailed comparison between theory and experiment for total capture, and for capture to H($2s$), H($2p$), and H($3s$) with moderate success for the latter. In the model calculation of Ref. [10] a two-center atomic orbital (TCAO) expansion of an independent many-electron wave function was constructed on the basis of a three-parameter phenomenological potential for argon fitted to experimentally determined average orbital energies. This work is expected to become inaccurate at higher collision energies where ionization dominates over capture, but it is unclear what effect the neglect of continuum channels has on detailed capture cross sections.

The total single-electron capture cross section as a function of energy displays agreement in shape, but overestimates the experimental cross sections at 8–200 keV collision energies by about 50%. For capture to excited states, the calculated energy-dependent cross sections display shapes which at higher energies are comparable with the experimental ones. However, rather substantial overestimations are found for these levels when compared with experiment.

Truly worrisome is the complete failure of the TCAO cal-

*Electronic address: tom.kirchner@tu-clausthal.de
†Electronic address: marko@yorku.ca
‡Electronic address: mkeim@th.physik.uni-frankfurt.de
§Electronic address: luedde@th.physik.uni-frankfurt.de

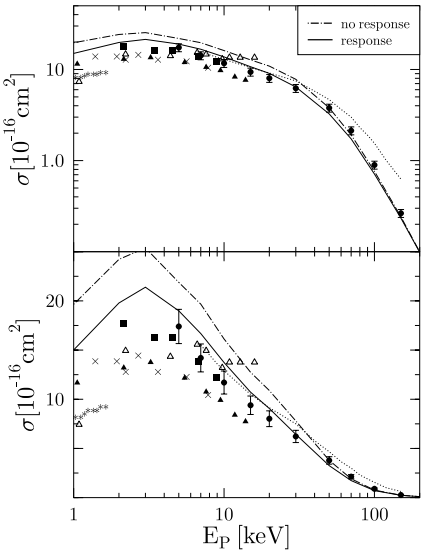

FIG. 1. Total cross section for single-electron capture as a function of impact energy for *p*-Ar collisions. Theory: present calculations with and without inclusion of the time-dependent target screening model (labeled as response and no response), and the two-center atomic orbital model of Ref. [10] (dotted line). Experiments: (▲) [11]; (●) [12]; (□) [13]; (×) [14]; (△) [15]; (*) [16].

culation for H($n=2$) capture at energies of 15 keV and below. Given that the authors mention the importance of electron correlation effects as a possible reason for the discrepancy, it is important to investigate the collision system using an *ab initio* IPM framework with a basis that is capable of describing the transition regime from adiabatic to faster collisions.

The main objective of this work is to provide an accurate calculation of capture to the K,L,M shells of hydrogen for energies in the 1–200 keV range. The case of *M*-shell capture is particularly interesting due to the uncertainties in the different experiments. The model is also tested on magnetic sublevel populations in H($2p$) capture, for which experimental data are available.

With the results presented in this paper we demonstrate that the experiments can largely be understood within the BGM-IPM. We do not repeat the details of the theoretical model, but refer the reader to the previous references and to Ref. [8] in particular. The latter work shows how the BGM-IPM deals with the many-electron aspects of the *p*-Ar collision system.

II. RESULTS AND DISCUSSION

In Ref. [8] we showed our net electron capture cross section, which corresponds to single-electron capture given that we ignore formation of the negative hydrogen ion. In Fig. 1 these data are extended to lower energies. The dual figure with the cross section shown both logarithmically and linearly allows us to display important trends at low and at high energies. Particularly noteworthy is the appearance of a distinct maximum at low energies, i.e., at 3 keV impact energy. The six experimental data sets when combined give an indication of a rather broad maximum in this range, but not one of them seems to have sufficient precision combined with energy range to provide a firm answer on this question. The work of Ref. [11] does indeed show a maximum at an energy of 3 keV, but the absolute values are low when compared to the data of Rudd and co-workers [12], which are considered accurate.

Our calculations for impact energies above 20 keV appear to be in good agreement with the data of Ref. [12] provided target response is included in the model for impact energies below 100 keV. At energies below 20 keV our data are, at best, in marginal agreement with this experiment, i.e., they overestimate the net capture cross section. The model calculation of Ref. [10] which does not include target response, obtains a very similar cross section for 10–30 keV, but then overestimates the data, reaching a factor-of-2 disagreement at 150 keV. This disagreement is most likely caused by the lack of representation of continuum channels which are in competition with capture to the ground state.

We emphasize that our total capture cross section peaks at 3 keV impact energy for both models. This is interesting insofar as the target response and no-response models incorporate changes in the Ar orbital energies during the collision which are caused by the reduction in screening following electron removal. Such changes can have a dramatic effect on capture probabilities, since energy level matchings between target and projectile orbitals will be affected. Nevertheless, we observe a reduction in cross section due to dynamical screening but no essential change in the shape of the cross section at lower energies. At high energies the results from both screening models merge, which indicates the collision time scale at which changes in the Ar(M) shell no longer influence the transition probabilities.

The maximum at 3 keV corresponds to a proton impact velocity of about $v_p \approx 0.34$ a.u. As shown below, the capture is predominantly from the Ar($3p_{|1|}$) orbitals into the ground state of hydrogen, which are energetically close. The maximum thus occurs at a velocity well below matching, and the cross section is rather large. If the capture was truly resonant a plateau in the cross section toward lower energies would be expected. One might therefore interpret the theoretical peak at 3 keV as the result of a near-resonant capture which eventually decreases at truly adiabatic energies when the mismatch in the energy levels and atomic potentials (as compared to truly resonant charge exchange) becomes important. In the frozen target potential model the Ar($3p$) orbitals are kept at the OPM (exchange only) eigenenergy of $\epsilon_{3p} = -0.59$ a.u., while the target response model increases the binding energy when the shell is depopulated. This results in a lowering of the capture cross section. The dynamics for the orbital propagation itself, however, remain the same, and the characteristic shape of the cross section is unchanged.

On theoretical grounds the present time-dependent density functional theory based calculation should allow one to calculate an accurate global capture cross section. We find a systematic overestimation of the experimental data by 10–40 % in the vicinity of the maximum and below depending on which experimental data set is used for comparison. This

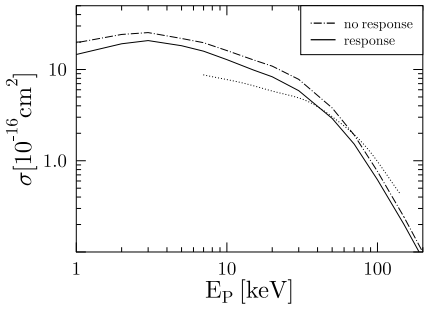

FIG. 2. Total cross section for single-electron capture to the hydrogen *K* shell as a function of impact energy for *p*-Ar collisions. Theory: present calculations with and without inclusion of the time-dependent target screening model (labeled as response and no response), and the two-center atomic orbital model of Ref. [10] (dotted line).

discrepancy would be reduced if an improved dynamic response model were implemented. For instance, dynamic screening of the projectile should reduce the amount of electron capture. However, we have not included such projectile response in the present calculation, because it would involve the creation of an unrealistic projectile hydrogen atom with fractional charge. Nevertheless, we can infer from a naive statistical evaluation of single- versus multiple-electron transfer that the net electron capture cross section as calculated here is overestimated (by perhaps up to 40%) due to the presence of unphysically large multiple-electron transfer contributions.

In Fig. 2 results are presented for our model with target response and with frozen target potential for capture to the hydrogen atom ground state, and are compared to the TCAO model calculation (no experiments are available for this channel). From a comparison with Fig. 1 it can be seen that capture to the ground state dominates the total capture cross section in our calculations. Again, there is no significant difference between our two models for the shape of this cross section, but a substantive disagreement with the TCAO data, especially at low energies. At high energies the TCAO model apparently overestimates the H($1s$) capture due to the lack of appropriate continuum channels.

At energies below 40 keV one observes a reduced H($1s$) capture cross section as compared to both of our models. This is surprising, as the total capture cross section from the TCAO calculation is in accord with our data from the target response model in this energy range. This implies that the TCAO calculation assigns a major fraction of total capture to the H($n=2$) channel at low energies, which is not supported by our calculations.

In order to shed some light on the discrepancy we can only comment that in this energy regime a reasonable representation of quasimolecular states becomes a requirement. The eigenenergies of the argon shells that contribute to the electron transfer process are not sufficiently different from the OPM eigenvalues which enter our frozen potential calculation. The close proximity of our calculations with and without target response for this channel suggests that the discrepancies between the two calculations have something to do with the flexibility of the basis to represent the time evolution of the Ar(M) orbitals in the presence of a slow nearby proton.

In order to clarify the situation we investigated at low energies the contributions of the Ar(M) subshells toward the charge transfer process [the Ar(K) and Ar(L) shells are energetically separated and make only tiny contributions, which are, however, calculated in the present work]. In Figs. 3(a)–3(c), the impact-parameter-dependent probabilities are shown for capture from Ar($3s$), Ar($3p_0$), and Ar($3p_1$) [which equals the corresponding probability from Ar($3p_{-1}$)], respectively, for three low energies. The Ar($3s$) orbital is bound more deeply than the energetically degenerate $3p$ orbitals. Obviously, the total charge transfer is dominated by capture from the orbital that extends furthest from the quantization axis, and that is bound most weakly. The charge transfer from Ar($3p_{\pm 1}$) occurs even at large impact parameters with a probability profile that does not change much with energy except for an increase with decreasing impact energy.

For capture from the Ar($3p_0$) level, we notice a less regular behavior when the impact energy is varied, and a confinement to smaller impact parameters in the charge transfer probability as the collision energy is decreased to 5 keV. The total capture probability is represented by the area under the respective curves and can be seen to decrease somewhat with decreasing energy, in contrast with the results for the sublevels with nonzero magnetic quantum numbers. Finally, for capture from the Ar($3s$) shell, we notice a marked decrease in transfer probability with decreasing energy with minor variations in the behavior of the impact-parameter-weighted probability.

In Fig. 4 we show our data for inclusive capture to the H($n=2$) states, i.e., to the hydrogen *L* shell. Above 10 keV they are in reasonable agreement with the experimental data, which were obtained by adding the experiments for capture

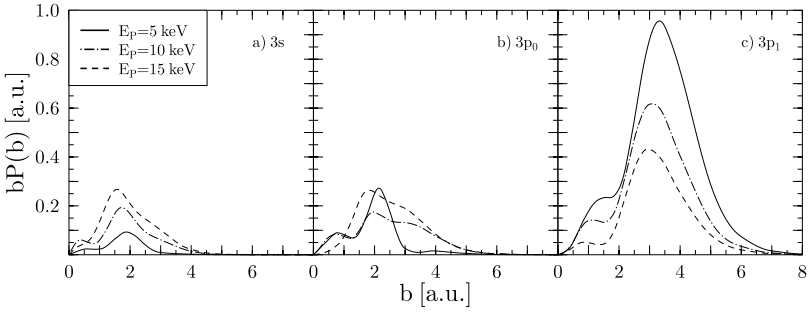

FIG. 3. Total probability for neutral hydrogen formation via electron capture from the Ar($3s$), Ar($3p_0$), and Ar($3p_1$) shells, respectively, as a function of impact parameter for *p*-Ar collisions. Calculations with inclusion of the time-dependent target screening model (response).

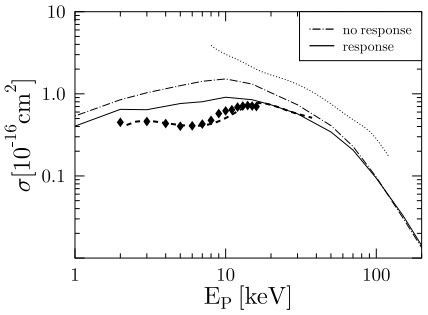

FIG. 4. Total cross section for single-electron capture to the hydrogen *L* shell as a function of impact energy for *p*-Ar collisions. Theory: present calculations with and without inclusion of the time-dependent target screening model (labeled as response and no response), and the two-center atomic orbital model of Ref. [10] (dotted line). Experiment: dashed line obtained by fitting to the experimental data summarized in Ref. [10]; (♦) [17].

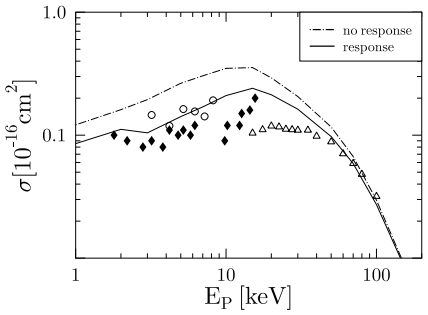

FIG. 5. Total cross section for single-electron capture to the hydrogen *M* shell as a function of impact energy for *p*-Ar collisions. Theory: present calculations with and without inclusion of the time-dependent target screening model (labeled as response and no response). Experiments: (♦) [17]; (△) calculated from Refs. [18,19]; (○) calculated from Refs. [20,21].

to H($2s$) and H($2p$). These theoretical data are not sensitive to Stark mixing and are therefore more reliable than the cross sections for specific H($2s$) or H($2p$) capture, which are discussed below.

For the 15–40 keV energy range, the agreement with experiment is perfect when target response is included. At lower energies the experimental data display a dip, which is a result of a superposition of a small depression in the H($2p$) capture cross section, which dominates *L*-shell capture, with a sharp dip in the H($2s$) capture channel. The present theoretical data do not follow this trend and overestimate the experiment by a factor of 2 at 7 keV. It would be of interest to find out to what extent dynamic screening in the vicinity of the projectile would lead to improvements, and to a more realistic shape in particular. The TCAO model calculation, on the other hand, is too large by a factor of 2 at energies above 30 keV, and continues to rise at lower energies to reach almost an order-of-magnitude discrepancy with experiment at 8 keV.

The situation admits the following interpretation. The present calculation with target response, which agrees with experiment for both the total capture and the *L*-shell capture, assigns most of the total capture to the *K* shell. The TCAO calculation obtains a reasonable total capture cross section, but this may well be fortuitous given that it obtains a significant part of the captured flux in the *L* shell. At energies below 10 keV it assigns about one-third of the total capture to H($n=2$), which is clearly not supported by the shell-specific experimental data.

The comparison of our results with and without target response can be used as an indication that it is not the frozen potential aspect of the TCAO model which is responsible for the steep rise in the *L*-shell capture cross section at low energies. On the other hand, it should be noted that the difference between our static and dynamic screening models is larger for this channel than for total capture. This implies that transfer to the more weakly bound hydrogen shells, which is energetically possible over a wider range of interatomic distances, is affected by the asymptotic behavior of the atomic potential.

Other differences between the TCAO model and the present BGM-IPM calculations could be responsible for the discrepancy. To understand whether the evolution of atomic orbitals within a TCAO basis is deficient at low energies it would be of interest to know to what extent the TCAO model of Ref. [10] can obtain a reasonable correlation diagram, i.e., whether one can diagonalize the electronic two-center Hamiltonian to within a few percent within the chosen basis. At energies of 10 keV and below, this ability to represent relevant molecular orbitals is deemed to be crucial in order to obtain the correct electron transfer probabilities.

The mentioned orbital propagation problem is an obvious point of concern at low collision energies, but one should not rule out the difference between the atomic models employed. It has been shown previously that atomic collision cross sections for many-electron targets can depend sensitively on the correct asymptotic behavior of the potential used in the IPM, and that the region where the potential approaches the characteristic $-1/r$ behavior is particularly important [1,2]. While this is probably less of an issue for capture to the H($n=1$) level which is bound relatively deeply, the capture to H($n=2$) (and higher levels) is more affected by regions where the atomic target potential is weak. Some clarification could be provided by TCAO model data for impact-parameter-dependent probabilities (cf. our Fig. 3) with an additional separation into H($n=1$) and H($n=2$) capture.

In Fig. 5 our results for H($n=3$) formation are compared to available experimental data. The low-energy results of Hughes *et al.* [18,19] and the higher-energy data of Dawson and Lloyd [20,21] are obtained by summing their respective H($3s$), H($3p$), and H($3d$) capture cross sections. It should be noted that at low energies the data have rather large error bars due to uncertainty in the H($3p$) formation cross section because of its small contribution toward Balmer-α emission. At the low-energy end of the data taken at higher energy, i.e., below 25 keV impact energy, the summed *M*-shell capture data of Ref. [19] are most likely to fall short due to the fact that the H($3p$) formation data seem to collapse. This explains at least in part why these data points are so low when compared to the overlapping data of Risley *et al.* [17] obtained with a different technique. When combining these re-

sults it is not entirely clear whether one should expect a maximum or a plateau at low energies over the range shown.

The theoretical data follow the experimental data at high energies rather closely. It should be noted that the absolute normalization of the experiments is uncertain to about 30%. In fact, the earlier H($3s$) formation data which are used to provide absolute normalizations for the other two channels were reported about 15–20 % higher in the early work [18].

Below about 50 keV we observe significant deviations between our calculations with and without target response, and the better model stays within reasonable proximity with the combined data sets—perhaps with an overestimation by about 30%. Our data show a broad maximum centered on 15 keV impact energy.

Some remarks are in order about the general shapes of the H($n=2$) and H($n=3$) capture cross sections as compared to the total capture and H($n=1$) capture cross sections, which peak at a projectile energy of $E_P=3$ keV. The present results display broad maxima for both *L*- and *M*-shell capture with center positions in the vicinity of 10–15 keV. The maximum is more pronounced in the *M*-shell case. The magnitudes of the *L*- and *M*-shell cross sections at 15 keV correspond to about 7% and 2% of the total capture, respectively. These observations indicate that captures to the *L* and *M* shells are somewhat similar processes, but drastically different from the *K*-shell capture. This is not surprising given the proximity of the H($1s$) and Ar($3p$) orbital energies on the one hand, and the closeness of the H($n=2$) and H($n=3$) energies in relation to their separation from Ar($3p$).

Concerning the capture to excited hydrogen states, and the *L* shell in particular there are discussions in the literature that apply to the lower-energy molecular orbital regime [22]. Based on total energy correlation diagrams involving the *p*-Ar and H-Ar^+ channels, it can be argued that the capture to the excited hydrogen levels follows a two-step process, in which the electron is first transferred to the *K* shell and then promoted to higher levels following curve crossings. The present calculations support this picture in the sense that an extremely large H($1s$) population is predicted, and that the single-electron adiabatic energy curves (which the BGM approach is able to calculate) also result in a realistic level of hydrogen excited states, which the TCAO calculation is not able to reproduce.

In Fig. 6 we show a comparison of the cross sections for capture to the H($2s$) and H($2p$) states. Calculations with and without target response are included. In order to take into account the Stark effect [mixing of the H($2s$) and H($2p_0$) states] the two-center Hamiltonian was diagonalized within the BGM basis. The quasimolecular states leading to the separated Stark eigenstates were identified from the adiabatic correlation diagram. A projection of the time-evolved BGM wave function onto these states (which were boosted to the projectile frame by an atomic translation factor) was then carried out.

The results for the H($2s$) population show that target response effects are significant at energies below 10 keV for this channel. At energies above 10 keV the data are in rather good agreement with the more recent data of Ref. [22], i.e., lower than a number of previous experiments by a factor of

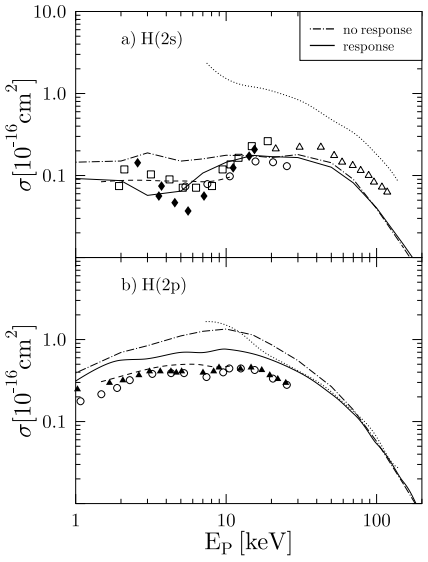

FIG. 6. Total cross section for single-electron capture to (a) the H($2s$) and (b) the H($2p$) states as a function of impact energy for *p*-Ar collisions. Theory: present calculations with and without inclusion of the time-dependent target screening model (labeled as response and no response) using projection onto traveling Stark states; two-center atomic orbital model of Ref. [10] (dotted line); molecular orbital (MO) calculation of Ref. [22] (dashed line). Experiments: (♦) [17]; (○) [22]; (△) [23]; (□) [24]; (▲) [25].

2. Below 10 keV impact energy the data with target response follow the experimentally observed reduction in cross section, while the frozen target potential calculation does not. We note that the correlated configuration-interaction molecular orbital expansion calculations of Ref. [22] do not show a minimum, but are rather close in height to our data.

For the capture to the H($2p$) state we observe substantial differences between our models with and without target response at energies below 40 keV. Our data even with target response are too high by a factor of 2 when compared with experiment for low to intermediate energies, but are mostly correct in shape. At low energies they also overestimate the correlated molecular-orbital calculations of Ref. [22]. The calculated H($2p$) formation cross section peaks at an energy of 10 keV where it is dominated by the equal H($2p_1$) and H($2p_{-1}$) channels, while H($2p_0$) formation is comparable to H($2s$) formation. However, at the highest energies shown the H($2p$) formation cross section is dominated by the H($2p_0$) channel.

Given that the inclusion of simple target response has led to a reduction of the H($2p_{\pm1}$) capture cross section by a factor of 3 in the vicinity of 10 keV impact energy, we expect that a more sophisticated dynamical screening model with a two-center geometry has potential for a further reduction of the H($2p$) transfer channels. It is interesting to observe that the strong sensitivity of the H($2p_{\pm1}$) capture channel to screening effects is in contrast with H($1s$) capture, which changes only at the 20% level in this energy range. One might argue that at these low to intermediate energies capture to H($1s$) happens to a large extent before the closest approach, and the promotion of the captured electron takes

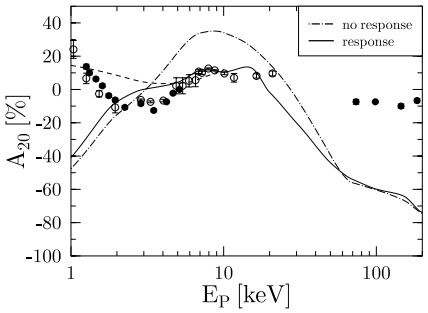

FIG. 7. Alignment parameter A_{20} for single-electron capture to the H($2p$) substates as a function of impact energy for p-Ar collisions. Theory: present calculations with and without inclusion of the time-dependent target screening model (labeled as response and no response); MO calculation of Ref. [22] (dashed line). Experiments: (●) [26]; (○) [27].

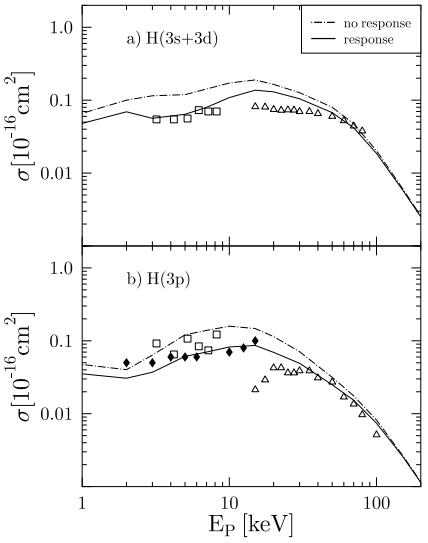

FIG. 8. Total cross section for single-electron capture to (a) the H($3s+3d$) and (b) the H($3p$) states as a function of impact energy for p-Ar collisions. Theory: present calculations with and without inclusion of the time-dependent target screening model (labeled as response and no response) using projection onto corresponding traveling Stark states (see text). Experiments: (♦) [17]; (△) [18,19]; (□) [20,21].

place shortly after closest approach such that the transfer to the H($2p_{\pm 1}$) states is strong. It is this second step of the excited-state capture mechanism which is changed significantly by the dynamical screening potential.

When comparing our results for state-selective $H(L)$ capture with the TCAO data, we notice that at energies above 20 keV the H($2p$) capture data of Ref. [10] agree rather closely with our data with target response. The H($2s$) capture data show a very similar energy dependence above 40 keV, but are higher by a factor of 4.

In order to investigate the details of H($2p$) capture we compare in Fig. 7 the alignment parameter A_{20}, which is calculated according to

$$A_{20}=\frac{\sigma_{2p_1}-\sigma_{2p_0}}{2\sigma_{2p_1}+\sigma_{2p_0}}, \tag{1}$$

with a possible range from -100% to 50%. From the available more recent experiments, it can be observed that generally speaking the alignment is small, with some oscillatory behavior around the line that corresponds to $\sigma_{2p_1}\approx\sigma_{2p_0}$. Between 2 and 20 keV our data with response are consistent with this trend, but share with the correlated many-electron MO calculations of Ref. [22] the tendency to miss some of the precise details. Nevertheless, these details and the behavior below 1 keV are usually discussed within the molecular curve-crossing models [22], and are common to several proton–rare-gas atom systems. Our calculations without response overestimate the alignment parameter at intermediate energies, i.e., dynamic target response is required in order to suppress H($2p_{|1|}$) formation.

At high energies our data are in marked disagreement with experiment. We find that H($2s$) and H($2p_0$) formation dominates the theoretical H(L)-shell capture cross section above 50 keV impact energy. The total capture cross section is dominated by H(K)-shell capture at high (as well as low and intermediate) energies. One possible mechanism for the strong favoring of the H($2p_0$) capture channel at high energies could again be a two-step process: it is plausible that electrons captured to the H($1s$) state are field excited by the receding Ar^+ ion during the second half of the collision. This excitation mechanism would strongly favor the state polarized along the internuclear axis.

It is worth noting that the entire Ar(M) shell contributes significantly to the transfer processes at higher energies. Charge transfer happens at small impact parameters in this regime, i.e., a spherically symmetric charge cloud is traversed by the projectile proton. Therefore, the authors of Ref. [22] also provide intuitive arguments for why the polarization parameter should be negative in this regime. A new measurement of the A_{20} parameter in the 20–200 keV energy range would be most welcome, because the current model calculation is considered to be most reliable in this collision regime.

In Fig. 8 we present cross sections for capture to sublevels of the M shell of hydrogen. The determination of these data is quite involved experimentally as well as theoretically. While capture to the $3p$ level of hydrogen can be analyzed directly by Ly(β) emission, the separation of the emission signals from the $3s$ and $3d$ decay is difficult: *both* states decay via Balmer(α) emission to H($2p$) and can be distinguished only by their lifetimes [17]. For this reason we present only capture cross sections for the combined channel H($3s+3d$).

Theoretically the situation is complicated by linear Stark mixing of the corresponding degenerate M-shell states of the outgoing hydrogen atom in the residual Coulomb potential of the partially ionized Ar ion. The six traveling Stark states representing the hydrogenic channels at finite separation are given by [17,28,29]

$$\begin{pmatrix} |1\rangle \\ |2\rangle \\ |3\rangle \end{pmatrix} = \begin{pmatrix} \psi(3,0,2,0) \\ \psi(3,1,1,0) \\ \psi(3,2,0,0) \end{pmatrix} = \begin{pmatrix} -1/\sqrt{3} & -1/\sqrt{2} & -1/\sqrt{6} \\ -1/\sqrt{3} & 0 & \sqrt{2/3} \\ -1/\sqrt{3} & 1/\sqrt{2} & -1/\sqrt{6} \end{pmatrix} \times \begin{pmatrix} \phi_{3s} \\ \phi_{3p_0} \\ \phi_{3d_0} \end{pmatrix},$$

$$\begin{pmatrix} |4\rangle \\ |5\rangle \end{pmatrix} = \begin{pmatrix} \psi(3,0,1,\pm 1) \\ \psi(3,1,0,\pm 1) \end{pmatrix} = \begin{pmatrix} -1/\sqrt{2} & -1/\sqrt{2} \\ -1/\sqrt{2} & 1\sqrt{2} \end{pmatrix} \begin{pmatrix} \phi_{3p_{\pm 1}} \\ \phi_{3d_{\pm 1}} \end{pmatrix},$$

$$|6\rangle = \psi(3,0,0,\pm 2) = -\phi_{3d_{\pm 2}}. \quad (2)$$

Cross sections for capture to $H(3p)$ are then obtained by summing the population of the Stark states $|2\rangle$ and $|4\rangle$, while the other Stark states contribute to $H(3s+3d)$.

Although capture to the M shell of hydrogen is smaller by a factor of 100 compared to electron transfer to the ground state, the agreement between experiment and theory is quite remarkable. This gives us some confidence in the validity of the approaches used in the present work.

III. CONCLUSIONS

In the present work we have demonstrated that shell-specific single-electron capture experiments for p-Ar collisions in the 1–200 keV energy range can largely be understood in an IPM framework, and that the BGM approach to orbital propagation is capable of providing the required details in Hilbert space in order to calculate reasonable total cross sections.

We offer the following comments as to why the model calculation of Ref. [10] fails for $H(n>1)$ capture, particularly below 20 keV, and why its agreement with the total capture cross section must be considered fortuitous at low energy. Our main concern is that the TCAO basis is simply inadequate at low energies. Secondary concerns are with the phenomenological potential model at intermediate r values. This distance range (before the $-1/r$ asymptotic behavior sets in) plays an important role at low energies because the impact-parameter-dependent probabilities for capture from the $Ar(3p_{\pm 1})$ orbitals extend over a large range.

Furthermore, we have shown that state-selective capture within the $H(n=2)$ shell can be calculated within a factor-of-2 accuracy at impact energies above 5 keV. It remains to be seen whether the inclusion of dynamic screening effects beyond the spherical target model—as employed in the present work—are responsible for the remaining discrepancies. Such nonspherical mean field contributions have recently been incorporated within the BGM approach in a calculation of antiprotons colliding with helium atoms [30]. If this theoretical avenue is exhausted and agreement with experiment is not found, electron correlation effects may indeed play a role for these one-electron transfer cross sections as suggested in Ref. [10].

An improved IPM calculation similar to [30] is desirable at low energies in order to shed light on the problem of the net capture cross section. A more satisfactory treatment would involve a true two-center screening model, but it is clear that conceptual difficulties are unavoidable in the mean-field approach. Future work will address these issues.

ACKNOWLEDGMENTS

This work was supported in part by the Natural Sciences and Engineering Research Council of Canada. We would like to thank E. Engel for providing us with the atomic structure calculations. We gratefully acknowledge support by the Frankfurt Center for Scientific Computing.

[1] T. Kirchner, L. Gulyás, H.J. Lüdde, A. Henne, E. Engel, and R.M. Dreizler, Phys. Rev. Lett. **79**, 1658 (1997).
[2] T. Kirchner, L. Gulyás, H.J. Lüdde, E. Engel, and R.M. Dreizler, Phys. Rev. A **58**, 2063 (1998).
[3] T. Kirchner, H.J. Lüdde, and R.M. Dreizler, Phys. Rev. A **61**, 012705 (2000).
[4] T. Kirchner, H.J. Lüdde, M. Horbatsch, and R.M. Dreizler, Phys. Rev. A **61**, 052710 (2000).
[5] T. Kirchner, M. Horbatsch, H.J. Lüdde, and R.M. Dreizler, Phys. Rev. A **62**, 042704 (2000).
[6] T. Kirchner and M. Horbatsch, Phys. Rev. A **63**, 062718 (2001).
[7] T. Kirchner, M. Horbatsch, and H.J. Lüdde, Phys. Rev. A **64**, 012711 (2001).
[8] T. Kirchner, M. Horbatsch, and H.J. Lüdde, Phys. Rev. A **66**, 052719 (2002).
[9] J.D. Talman and W.F. Shadwick, Phys. Rev. A **14**, 36 (1976).
[10] A. Amaya-Tapia, H. Martínez, R. Hernańdez-Lamoneda, and C.D. Lin, Phys. Rev. A **62**, 052718 (2000).
[11] S.K. Allison, Rev. Mod. Phys. **30**, 1137 (1958).
[12] M.E. Rudd, R.D. DuBois, L.H. Toburen, C.A. Ratcliffe, and T.V. Goffe, Phys. Rev. A **28**, 3244 (1983).
[13] J. Williams and D.N.F. Dunbar, Phys. Rev. **149**, 62 (1966).
[14] B.J.H. Stedeford and J.B. Hasted, Proc. R. Soc. London, Ser. A **227**, 466 (1955).
[15] Y.S. Gordeev and M.N. Panov, Zh. Tekh. Fiz. **34**, 857 (1964) [Sov. Phys. Tech. Phys. **9**, 656 (1964)].
[16] Z.Z. Latypov and A.A. Shaporenko, Zh. Tekh. Fiz. **46**, 2178 (1976) [Sov. Phys. Tech. Phys. **21**, 1277 (1976)].
[17] J.S. Risley, F. de Heer, and C.B. Kerkdijk, J. Phys. B **11**, 1759 (1978).
[18] R.H. Hughes, H.R. Dawson, B.M. Doughty, D.B. Kay, and C.A. Stigers, Phys. Rev. **146**, 53 (1966).
[19] R.H. Hughes, C.A. Stigers, B.M. Doughty, and E.D. Stokes, Phys. Rev. A **1**, 1424 (1970).
[20] H.R. Dawson and D.H. Loyd, Phys. Rev. A **9**, 166 (1974).
[21] H.R. Dawson and D.H. Loyd, Phys. Rev. A **15**, 43 (1977).
[22] G. Tepehan, B. Siegmann, H. Madeheim, R. Hippler, and M. Kimura, J. Phys. B **27**, 5527 (1994).
[23] R.H. Hughes, E.D. Stokes, S.-S. Choe, and T. King, Phys. Rev. A **4**, 1453 (1971).

[24] D. Jaecks, B. van Zyl, and R. Geballe, Phys. Rev. **137**, A340 (1965).
[25] D. Pretzer, B. van Zyl, and R. Geballe, Phys. Rev. Lett. **10**, 340 (1963).
[26] R. Hippler, W. Harbich, M. Faust, H. Lutz, and L. Dubé, J. Phys. B **19**, 1507 (1986).
[27] P. Teubner, W. Kauppila, W. Fite, and R. Girnius, Phys. Rev. A **2**, 1763 (1970).
[28] H. Bethe and E. Salpeter, *Quantum Mechanics of One- and Two-Electron Systems* (Springer, Berlin, 1957), Chap. 51.
[29] H. Friedrich, *Theoretical Atomic Physics* (Springer, Berlin, 1998), Chap. 3.4.
[30] M. Keim, A. Achenbach, H. Lüdde, and T. Kirchner, Phys. Rev. A **67**, 062711 (2003).